Note added in proof: After the present work was accepted for publication, an independent study of the magnetic susceptibility of $Dy_2Ti_2O_7$ was published by Matsuhira *et al.*[31], offering a somewhat different interpretation of the behaviour. □

Methods

We studied polycrystalline samples of $Dy_2Ti_2O_7$, prepared from high-purity Dy_2O_3 and TiO_2 powders mixed in stoichiometric proportion and heated at 1,350 °C in air for a period of one week with intermediate grindings. The samples were shown to be single-phase pyrochlore type by powder X-ray diffraction. We have also studied a single crystal grown in a travelling floating zone mirror furnace, and obtain qualitatively equivalent data.

The d.c. susceptibility measurements were performed on a Quantum Design MPMS SQUID magnetometer. The a.c. susceptibility measurements were made with a Quantum Design PPMS system with the ACMS option. The data were independent of the amplitude of the excitation field between 10^{-4} and 10^{-3} T, and the frequency independence of the susceptometer was verified with a DyO calibration sample. As the Dy spins are highly anisotropic in $Dy_2Ti_2O_7$, these measurements probe the vast majority of the spins in our polycrystalline samples, with the exception of those whose easy axis is directed perpendicular to the applied field.

Received 14 May; accepted 20 July 2001.

1. Ramirez, A. P. in *Handbook of Magnetic Materials* Vol. 13 (ed. Buschow, K. J. H.) 423–520 (Elsevier Science, Amsterdam, 2001).
2. Onuchic, J. N., Luthey-Schulten, Z. & Wolynes, P. G. Theory of protein folding: The energy landscape perspective. *Ann. Rev. Phys. Chem.* **48,** 545–600 (1997).
3. Hopfield, J. J. Neurons with graded response have collective computational properties like those of two-state neurons. *Proc. Natl Acad. Sci.* **81,** 3088–3092 (1984).
4. Pauling, L. *The Nature of the Chemical Bond* 301–304 (Cornell Univ. Press, Ithaca, New York, 1945).
5. Petrenko, V. F. & Whitworth, R. W. *Physics of Ice* (Clarendon, Oxford, 1999).
6. Harris, M. J., Bramwell, S. T., McMorrow, D. F., Zeiske, T. & Godfrey, K. W. Geometrical frustration in the ferromagnetic pyrochlore $Ho_2Ti_2O_7$. *Phys. Rev. Lett.* **79,** 2554–2557 (1997).
7. Harris, M. J., Bramwell, S. T., Holdsworth, P. C. W. & Champion, J. D. M. Liquid-gas critical behaviour in a frustrated pyrochlore ferromagnet. *Phys. Rev. Lett.* **81,** 4496–4499 (1998).
8. Bramwell, S. T. & Harris, M. J. Frustration in Ising-type spin models on the pyrochlore lattice. *J. Phys. Condens. Matter* **10,** L215–L220 (1998).
9. Ramirez, A. P., Hayashi, A., Cava, R. J., Siddharthan, R. & Shastry, B. S. Zero-point entropy in 'spin ice'. *Nature* **399,** 333–335 (1999).
10. Harris, M. J. Taking the frustration out of ice. *Nature* **399,** 311–312 (1999).
11. Siddharthan, R. *et al.* Ising pyrochlore magnets: low-temperature properties, "ice rules," and beyond. *Phys. Rev. Lett.* **83,** 1854–1857 (1999).
12. den Hertog, B. C., Melko, R. G. & Gingras, M. J. P. Long range order at low temperature in dipolar spin ice. Preprint cond-mat/0009225 at ⟨http://xxx.lanl.gov⟩ (2000).
13. Gingras, M. J. P. & den Hertog, B. C. Origin of spin ice behavior in Ising pyrochlore magnets with long range dipole interactions: an insight from mean-field theory. Preprint cond-mat/0012275 at ⟨http://xxx.lanl.gov⟩ (2000).
14. Kawada, S. Dielectric anisotropy in ice Ih. *J. Phys. Soc. Jpn* **44,** 1881–1886 (1978).
15. Haida, O., Matsuo, T., Hiroshi, S. & Seki, S. Calorimetric study of the glassy state X. Enthalpy relaxation at the glass-transition temperature of hexagonal ice. *J. Chem. Thermodyn.* **6,** 815–825 (1974).
16. Giaque, W. F. & Stout, J. W. The entropy of water and the third law of thermodynamics. The heat capacity of ice from 15K to 273K. *J. Am. Chem. Soc.* **58,** 1144–1150 (1936).
17. Rosenkranz, S. *et al.* Crystal-field interaction in the pyrochlore magnet $Ho_2Ti_2O_7$. *J. Appl. Phys.* **87,** 5914–5916 (2000).
18. Ramirez, A. P., Espinosa, G. P. & Cooper, A. S. Strong frustration and dilution enhanced order in a quasi-2D spin glass. *Phys. Rev. Lett.* **64,** 2070–2073 (1990).
19. Gardner, J. S. Glassy statics and dynamics in the chemically ordered pyrochlore anti-ferromagnet $Y_2Mo_2O_7$. *Phys. Rev. Lett.* **83,** 211–215 (1999).
20. Schiffer, P. *et al.* Frustration induced spin freezing in a site-ordered magnet—gadolinium gallium garnet. *Phys. Rev. Lett.* **74,** 2379–2382 (1995).
21. Wills, A. S. Long range ordering and representational analysis of the jarosites. *Phys. Rev. B* **63,** 064430-1–064430-12 (2001).
22. Mydosh, J. A. *Spin Glasses: An Experimental Introduction* (Taylor & Francis, London, 1993).
23. Reich, D. H., Rosenbaum, T. F. & Aeppli, G. Glassy relaxation without freezing in a random dipolar-coupled Ising magnet. *Phys. Rev. Lett.* **59,** 1969–1972 (1987).
24. Fiorani, D., Tholence, J. & Dorman, J. L. Magnetic properties of small ferromagnetic particles (Fe-Al_2O_3 granular thin films): Comparison with spin glass properties. *J. Phys. C* **19,** 5495–5507 (1986).
25. Casimir, H. B. G. & du Pré, F. K. Note on the thermodynamic interpretation of paramagnetic relaxation phenomena. *Physica* **5,** 507–511 (1938).
26. Dirkmaat, A. J. *et al.* Frequency-dependence of the ac susceptibility in the random anisotropy system $Dy(P_{1-x}V_x)O_4$. *Phys. Rev. B* **36,** 352–359 (1987).
27. Huser, D., Wenger, L. E., van Duyneveldt, A. J. & Mydosh, J. A. Dynamical behavior of the susceptibility around the freezing temperature in (Eu,Sr)S. *Phys. Rev. B* **27,** 3100–3103 (1983).
28. Dekker, C., Arts, A. F. M., de Wijn, H. W., van Duyneveldt, A. J. & Mydosh, J. A. Activated dynamics in a two-dimensional Ising spin glass: $Rb_2Cu_{1-x}Co_xF_4$. *Phys. Rev. B* **40,** 243–251 (1989).
29. Bramwell, S. T. *et al.* Spin correlations in $Ho_2Ti_2O_7$: A dipolar spin ice system. *Phys. Rev. Lett.* **87,** 047205-1–047205-4 (2001).
30. Matsuhira, K., Hinatsu, Y., Tenya, K. & Sakakibara, T. Low temperature magnetic properties of frustrated pyrochlore ferromagnets $Ho_2Sn_2O_7$ and $Ho_2Ti_2O_7$. *J. Phys. Condens. Matter* **12,** L649–L656 (2000).
31. Matsuhira, K., Hinatsu, Y. & Sakakibara, T. Novel dynamical magnetic properties in the spin ice compound $Dy_2Ti_2O_7$. *J. Phys. Condens. Matter* **13,** L737 (2001).

Acknowledgements

We thank D.A. Huse, T. Rosenbaum and J. Banavar for discussions. This work was supported by the Army Research Office.

Correspondence and requests for materials should be addressed to P.S. (e-mail: schiffer@phys.psu.edu).

Fluidity of water confined to subnanometre films

Uri Raviv, Pierre Laurat* & Jacob Klein*

Weizmann Institute of Science, Rehovot 76100, Israel

The fluidity of water in confined geometries is relevant to processes ranging from tribology to protein folding, and its molecular mobility in pores and slits has been extensively studied using a variety of approaches[1–6]. Studies in which liquid flow is measured directly suggest that the viscosity of aqueous electrolytes confined to films of thickness greater than about 2–3 nm remains close to that in the bulk[7–9]; this behaviour is similar to that of non-associative organic liquids confined to films thicker than about 7–8 molecular layers[8,10,11]. Here we observe that the effective viscosity of water remains within a factor of three of its bulk value, even when it is confined to films in the thickness range 3.5 ± 1 to 0.0 ± 0.4 nm. This contrasts markedly with the behaviour of organic solvents, whose viscosity diverges when confined to films thinner than about 5–8 molecular layers[10–15]. We attribute this to the fundamentally different mechanisms of solidification in the two cases. For non-associative liquids, confinement promotes solidification by suppressing translational freedom of the molecules[11,15–18]; however, in the case of water, confinement seems primarily to suppress the formation of the highly directional hydrogen-bonded networks associated with freezing[1,3].

Highly purified water (conductivity water, see Fig. 1) was introduced between curved mica surfaces in a surface-force balance (SFB) capable of measuring both normal and lateral surface forces with extreme sensitivity and resolution[11]. Normal surface forces $F_n(D)$, where D is separation, were measured as a control both at the start and at several points during experiments, and are shown in Fig. 1. They reveal the long-ranged repulsion associated with the presence of charge on the mica surfaces, arising from the loss of potassium ions to solution. No indication of short-ranged hydration repulsion is seen, and, in agreement with earlier work[19], the surfaces jump from separations $D = D_j = 3.5 \pm 1$ nm into flat adhesive contact, $D = D_0 = 0.0 \pm 0.4$ nm, as revealed by the position and shape of the optical interference fringes in the SFB. (As the size of a water molecule is roughly 0.25 nm, the presence of, at most, one monolayer of water per mica surface following adhesive contact cannot be ruled out within our resolution.) The spontaneous inward motion, which occurs in a single monotonic jump from D_j to D_0, is driven by van der Waals attraction between the surfaces overcoming the double-layer repulsion. It is due to an instability expected whenever $|(\partial F_n/\partial D)| > K_n$, where K_n is the constant of the normal spring (top inset to Fig. 2). The results reported here are based on seven separate experiments (using different pairs of mica sheets) as well as different contact points within experiments.

The surfaces were separated and enabled to approach slowly from

* Present addresses: Service Recherche Technologies et Systèmes, LEGRAND SA 128, avenue de Lattre de Tassigny, 87045 Limoges Cedex, France (P.L.); and at Physical and Theoretical Chemistry Laboratory, South Parks Road, Oxford OX1 3QZ, UK (J.K.).

large separations, $D > 10$ nm, under thermal drift (this varies slightly but was typically 0.03 nm s^{-1}), while we recorded the lateral motion of the lower surface due to ambient vibrations, as shown in trace A of Fig. 2. Once the surfaces jump (from $D = D_j$) into adhesive contact, the noise level drops markedly. The period τ_j over which the jump occurs is estimated from observation of the interference fringes to be in the range 0.2–0.5 s, in line with earlier estimates[20]. In a different type of measurement, with the surfaces initially separated, the upper mica surface was made to move laterally back-and-forth parallel to the lower one at velocity v_s (trace B in Fig. 2). The shear forces F_s transmitted across the intersurface gap are simultaneously recorded as the surfaces approach under slow thermal drift. No shear forces greater than the noise-limited sensitivity δF_s (± 20 nN, lower left inset) can be observed down to $D = D_j$, when the jump into adhesive contact results in rigid coupling between the surfaces (trace C, and lower right inset). In all cases the behaviour described was fully reproducible on subsequent separations and approaches. An upper limit η^u_{eff} on the effective shear viscosity may be estimated from the magnitude of the shear force $F_s < \delta F_s$ transmitted across the gap[11] as $\eta^u_{eff} = (\partial F_s/\partial D)/[(16\pi/5)R(v_s/D)]$. This yields $\eta^u_{eff} < 0.1$ Pa s, just before the jump in at $D = D_j = 2.4 \pm 0.3$ nm for the run shown in Fig. 2. Although much larger than the viscosity of bulk water, this value is an upper limit and is consistent with earlier reports[7–9] on the fluidity of aqueous salt solutions confined to films thicker than about 2 nm. It is particularly noteworthy that during the jump itself, as clearly seen in the magnified region of trace C, the magnitude of F_s remains within the noise level right up to the point at which the surfaces come into rigid adhesive contact. This suggests that the viscosity of the water when confined—during the jump itself—to layers of thickness between 3.5 ± 1 nm and 0 ± 0.4 nm remains well within this upper limit η^u_{eff}.

More stringent limits on the viscosity of the water when it is confined to such subnanometre films ($D < 2$–3 nm), down to the final few ångstroms, may be set by considering in detail the processes occurring as the surfaces jump from D_j to adhesive contact. In this

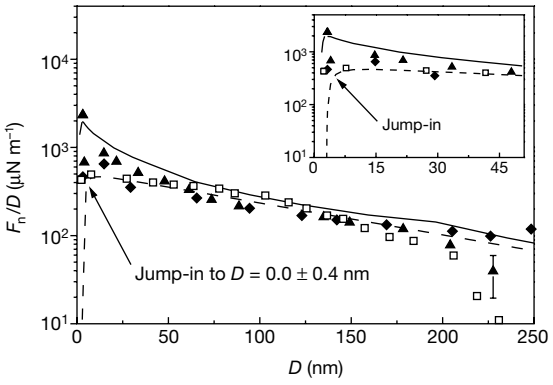

Figure 1 Normal surface interaction measurements used to control for the water and surface characteristics in our experiments. Force (F_n/R) against distance (D) profile between curved mica surfaces (mean radius of curvature $R = 1$ cm) across conductivity water at 23 ± 1 °C. The solid curve is from the study on conductivity water by Pashley[19], and the broken line corresponds to an exponential decay length (Debye length) of 120 ± 20 nm, corresponding to (6.4 ± 1) × 10^{-6} M 1 : 1 salt concentrations and a surface potential of 130 ± 20 mV. A solid–liquid surface tension -2.6 ± 0.4 mN m^{-1} can be deduced from the force required for pull-off from adhesive contact. These values are slightly lower than earlier reports[19]. The zero of the surface separation axis, $D = 0$ in water, is at a position -0.5 ± 0.3 nm with respect to air contact between the surfaces, based on measurements at eight contact positions from seven different experiments, showing that a water-soluble layer coats the mica surfaces in air before addition of the conductivity water. Comparison with earlier studies[20,28] indicates that the adhesive contact separation in water in our experiments (D_0) is, within our resolution, the contact separation of the mica lattice planes in the uncleaved crystals. Purification: tap water treated with activated charcoal was passed through a Millipore purification system (RiOs™ followed by a Milli-Q™ Gradient stage), yielding water with specific resistivity greater than 18.2 MΩ (corresponding to less than 4 × 10^{-7} M 1 : 1 salt concentration) and total organic content less than 4 p.p.b. The higher ion concentration indicated by the measured Debye length is probably due to ions leached from the glassware and to dissolved CO_2. Different symbols correspond to different experiments. The inset shows the jump-in regime on an expanded scale.

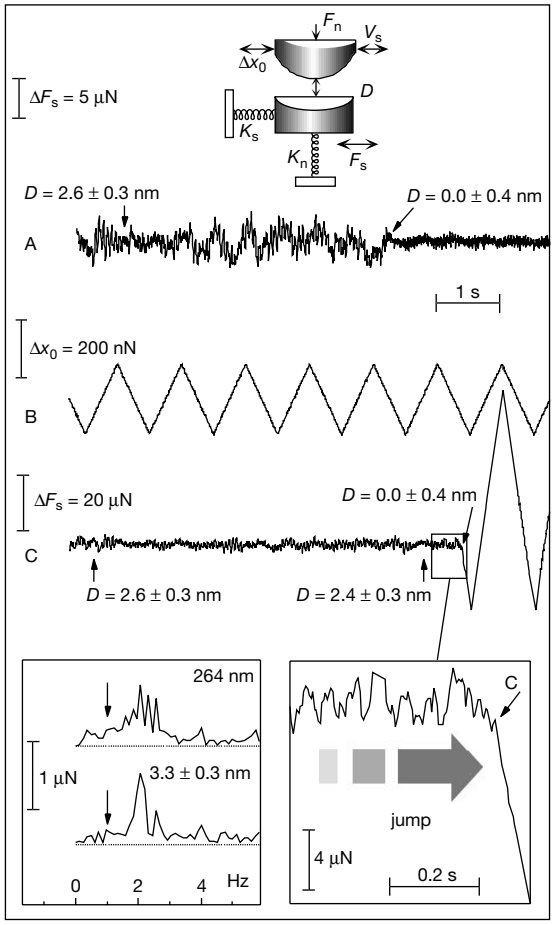

Figure 2 Measurements of the shear forces between sliding mica surfaces across water during approach to contact. The top cartoon shows schematically the relative motion, separation and direction of the forces measured between the two crossed cylindrical surfaces of mica in the surface force balance[11] (indicating the shear and normal force springs of respective constants K_s and K_n). The top surface may be moved laterally in the $\pm\Delta x_0$ direction by means of a sectored piezoelectric tube (PZT), while the distortion Δx of the shear spring gives $F_s = K_s\Delta x$ and is monitored directly from changes in an air-gap capacitor. Trace A shows the noise in F_s arising from ambient vibrations as the surfaces approach each other slowly (at about 0.03 nm s^{-1}) under thermal drift and jump into contact to $D = D_0 = 0.0 \pm 0.4$ nm (arrow). Trace B shows the back-and-forth lateral motion applied to the top mica surface by the sectored PZT as the surfaces drift slowly towards each other. Trace C shows the corresponding shear force F_s transmitted between the surfaces: it is indistinguishable from the noise until they have jumped together into adhesive contact (arrow and point C on the expanded lower right inset), following which $F_s = K_s\Delta x = K_s\Delta x_0$ as the two surfaces move in tandem. Frequency analysis (lower left inset) reveals that the magnitude of F_s at the frequency of the lateral drive motion (1 Hz, indicated by arrow) for a surface separation $D = 3.3$ nm is essentially identical to its value at large separations ($D = 264$ nm), both being due to bending of the connecting PZT wires[11] and to ambient noise rather than to any transmitted shear force F_s. Their difference (0 ± 20 nN, averaged over several experiments) may be taken as the noise-limited sensitivity δF_s in measuring the shear force between the surfaces.

regime, if we treat the effective geometry of the curved surfaces as that of a sphere of radius R approaching a flat surface, the equation of motion is to a good approximation

$$M(\mathrm{d}^2D/\mathrm{d}t^2) + 6\pi R^2\eta_{\mathrm{eff}}[(\mathrm{d}D/\mathrm{d}t)/D] = F_{\mathrm{vdW}}(D) - K_{\mathrm{n}}(D_{\mathrm{j}} - D) \quad (1)$$

where M is the effective mass of the moving mica surface and its mounting, the second term on the left is the Reynolds hydrodynamic resistance[21] to the approach of a sphere to a flat across a medium of viscosity η_{eff}, and we ignore the very small change in the double-layer interaction in the interval $\{D_{\mathrm{j}}, D_0\}$. In this surface separation regime the dominant force driving the approach of the surfaces is the van der Waals dispersive attraction, $F_{\mathrm{vdW}}(D) = AR/6D^2$, where $A = -2 \times 10^{-20}$ J is the relevant Hamaker constant. It is readily shown that in the conditions of our experiments the inertial term and that (in K_{n}) due to the spring bending are negligible compared with the other terms. The time τ_{j} for the surfaces to jump from D_{j} to D_0 is thus

$$\tau_{\mathrm{j}}(\eta_{\mathrm{eff}}, D_{\mathrm{j}}, D_0) = \int_{D_0}^{D_{\mathrm{j}}} \frac{36\pi R\eta_{\mathrm{eff}}D}{A}\,\mathrm{d}D = \left(\frac{18\pi R\eta_{\mathrm{eff}}}{A}\right)\left(D_{\mathrm{j}}^2 - D_0^2\right) \quad (2)$$

The variation of τ_{j} with D_0 is shown in the inset to Fig. 3 for $D_{\mathrm{j}} = 3.5$ nm and $\eta_{\mathrm{eff}} = \eta_{\mathrm{bulk}} = 0.86 \times 10^{-3}$ Pa s, the viscosity of bulk water at 23 °C. The vertical shaded band in Fig. 3 shows the range of experimental τ_{j} values; also shown, for values of the jump separation in the range $D_{\mathrm{j}} = (2.5\text{–}4.5)$ nm, is the implicit relation (from equation (2)) between the jump time to $D_0 = 0$ and the effective viscosity η_{eff}. The range of η_{eff} where $\tau_{\mathrm{j}}(\eta_{\mathrm{eff}}, D_{\mathrm{j}}, 0)$ overlaps the shaded band, shown by horizontal dotted lines, thus defines the range of effective viscosities that correspond to the experimental jump times. This shows that the viscosity of water confined to films of thickness in the range 3.5 ± 1 nm down to 0.0 ± 0.4 nm is within a factor of 3 or so in either direction of the viscosity of bulk water η_{bulk}. The uncertainty arises from the scatter in the values of the jump distance D_{j} and the jump time τ_{j}. It is of interest that the viscosity corresponding to the mid-range of both D_{j} (3.5 nm) and the experimental τ_{j} (0.35 s), indicated as the filled square in Fig. 3, is close to that of bulk water. A more detailed consideration shows that the magnitude of η_{eff} remains within or close to this range at all film thicknesses throughout the jump into contact. We note also that the effective maximal shear rates during our measurements vary from about $10^2\ \mathrm{s}^{-1}$ in the absence of applied lateral motion before the jump-in (Fig. 2a), to about $10^4\ \mathrm{s}^{-1}$ during the jump-in itself[22]. Within our resolution, the effective viscosity of the confined water is similar at these different shear rates, indicating that its behaviour is Newtonian within this range.

This result represents a direct evaluation of the viscosity of water confined to subnanometre films, and is in remarkable contrast to the properties of similarly confined non-associative organic liquids. Experiments and simulations show that both water and organic liquids undergo layering near smooth solid surfaces, and that both retain their bulk fluidity when confined to films thicker than some 8–10 molecular layers[6–11,14,15,23]. Simple non-associative liquids, however, are solid-like or have diverging viscosities when they are confined to films less than 5–8 molecular layers thick[10–15], whereas the viscosity of water, as revealed here, remains comparable to its bulk value even within films down to one or two monolayers thick[24].

Why does water behave so differently from organic liquids confined to correspondingly thin films between solid surfaces? Models for non-associative liquids (which include most organic solvents) suggest that, as the confinement increases, the translational entropy available to the molecules decreases to the point at which it becomes thermodynamically favourable for them to condense to an ordered phase[15–18], with consequent solid-like behaviour even at temperatures where the bulk is disordered and fluid. The origin of solidification in water is rather different: the formation of ice with its highly directional hydrogen-bond lattice[1,3] is thermodynamically favoured despite the large accompanying loss of the hydrogen-bond entropy available in liquid water. Now we expect that the confining surfaces locally must induce translational order (because they reduce the translational entropy of adjacent water molecules much as for non-associative molecules). Moreover, the mica surface is hydrophilic and fairly commensurate with water[25] and this should provide an additional surface ordering mechanism. Thus our observation that the confined water nonetheless retains its bulk fluidity presumably implies that these ordering effects cannot

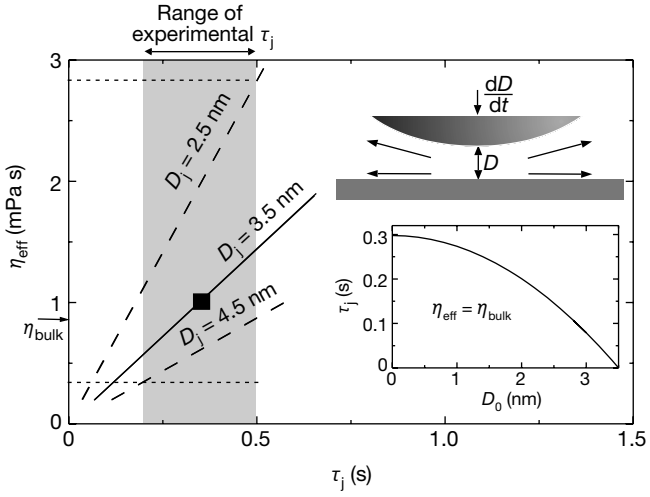

Figure 3 Evaluation of the effective viscosity of confined water from the jump-in data (Fig. 2). The cartoon (top right) illustrates the jump-in driven by van der Waals attraction and opposed by the hydrodynamic force resulting from the expulsion of the viscous liquid from between the surfaces. The inset (lower right) shows how, for an effective viscosity $\eta_{\mathrm{eff}} = \eta_{\mathrm{bulk}} = 0.86$ mPa s (the viscosity of bulk water at 23 °C), the jump time τ_{j} varies with jump distance for a jump commencing at $D_{\mathrm{j}} = 3.5$ nm, according to equation (2). The main figure shows the effective viscosity η_{eff} of the liquid being squeezed out of the gap corresponding to the jump time to contact τ_{j}, for three values of the jump distance D_{j}: the mid-range value 3.5 nm (solid line) and the two extremes from which jumps occurred, $D_{\mathrm{j}} = 2.5$ and 4.5 nm (broken lines). The shaded vertical band is the range of experimentally determined τ_{j}, so that the range of effective viscosity η_{eff} of the confined water films in the thickness interval $(3.5 \pm 1$ nm, 0), which corresponds to the experiments, is defined (horizontal dotted lines) by the overlap of the broken lines with the shaded band. This possible range of values is within a factor of 3 or so either side of η_{bulk}; its mid-range value with respect to D_{j} and τ_{j}, indicated as a solid square, is close to η_{bulk} itself.

overcome the network entropy of the hydrogen bonding in the fluid state. Equivalent differences are found also in the bulk: above a critical density or pressure, non-associative liquids spontaneously go to an ordered phase, whereas it is well known that pressure promotes melting of ice. The effect of confinement is in some measure equivalent to a pressure (or density) increase relative to the unconfined bulk, due to the attraction exerted on the solvent molecules by the confining walls[26]; such a density increase opposes any tendency to freeze. This suggests that the fluidity of water even under the most severe confinement is directly related to the well-known anomalous density decrease of water on freezing, as well as to the considerable supercooling of water possible near surfaces and in small droplets[1].

This persistent fluidity clearly has interesting consequences for many phenomena where confined water is implicated. It should be emphasized, however, that our present study examined conductivity water, where the ion concentration (of the order of 10^{-6} M) is lower by many orders of magnitude than is commonly found in nature or technology and where the confining surfaces attract each other at subnanometre separations. It is possible that where the surfaces are covered with hydrated ions (as for the case of mica across electrolytes at higher salt concentrations), and thus repel at such separations, the behaviour of the confined aqueous films may be different[24,27]. □

Received 6 April; accepted 24 June 2001.

1. Clifford, J. in *Water in Disperse Systems* (ed. Franks, F.) 75–132 (Plenum, New York and London, 1975).
2. Drake, J. M. & Klafter, J. Dynamics of confined molecular systems. *Phys. Today* **43,** 43–45 (1990).
3. Bellissent-Funel, M.-C. & Dore, J. C. (eds) *Hydrogen Bond Networks* (NATO ASI Series) (Kluwer Academic, Dordrecht, 1994).
4. Xia, X., Perera, L., Essmann, U. & Berkowitz, M. L. The structure of water at platinum/water interfaces: Molecular dynamics computer simulations. *Surf. Sci.* **335,** 401–415 (1995).
5. Meyer, M. & Stanley, H. E. Liquid–liquid phase transition in confined water: A Monte Carlo study. *J. Phys. Chem. B* **103,** 9728–9730 (1999).
6. Gallo, P., Rovere, M. & Spohr, E. Glass transition and layering effects in confined water: A computer simulation study. *J. Chem. Phys.* **113,** 11324–11335 (2000).
7. Roberts, A. D. & Tabor, D. The extrusion of liquids between highly elastic solids. *Proc. R. Soc. Lond. A* **325,** 323–345 (1971).
8. Israelachvili, J. N. Measurement of the viscosity of liquids in very thin films. *J. Colloid Interf. Sci.* **110,** 263–271 (1986).
9. Horn, R. G., Smith, D. T. & Haller, W. Surface forces and viscosity of water measured between silica sheets. *Chem. Phys. Lett.* **162,** 404–408 (1989).
10. Granick, S. Motions and relaxations of confined liquids. *Science* **253,** 1374–1379 (1991).
11. Klein, J. & Kumacheva, E. Simple liquids confined to molecularly thin layers. I. Confinement-induced liquid to solid phase transitions. *J. Chem. Phys.* **108,** 6996–7009 (1998).
12. Rhykerd, C. L., Schoen, M., Diestler, D. J. & Cushman, J. H. Epitaxy in simple classical fluids in micropores and near-solid surfaces. *Nature* **330,** 461–463 (1987).
13. Israelachvili, J., McGuiggan, P. M. & Homola, A. M. Dynamic properties of molecularly thin liquid-films. *Science* **240,** 189–191 (1988).
14. Thompson, P. A., Robbins, M. O. & Grest, G. S. Structure and shear response in nanometer-thick films. *Isr. J. Chem.* **35,** 93–106 (1995).
15. Gao, J., Luedtke, W. D. & Landman, U. Layering transitions and dynamics of confined liquid films. *Phys. Rev. Lett.* **79,** 705–708 (1997).
16. Chandler, D., Weeks, J. D. & Anderson, H. C. Van der Waals picture of liquids, solids and phase transformations. *Science* **220,** 787–794 (1983).
17. Tkachenko, A. & Rabin, Y. Effect of boundary conditions in fluctuations and solid-liquid transition in confined films. *Langmuir* **13,** 7146–7150 (1997).
18. Weinstein, A. & Safran, S. A. Surface and bulk ordering in thin films. *Europhys. J.* **42,** 61–64 (1998).
19. Pashley, R. M. Hydration forces between mica surfaces in aqueous electrolyte solutions. *J. Colloid Interf. Sci.* **80,** 153–162 (1980).
20. Israelachvili, J. N. & Adams, G. E. Measurement of forces between two mica surfaces in aqueous electrolyte solutions in the range 0–100 nm. *J. Chem. Soc. Faraday Trans. I* **79,** 975–1001 (1978).
21. Happel & Brenner, H. *Low Reynolds Number Hydrodynamics* (Prentice Hall, Englewood Cliffs, 1965).
22. Chan, D. Y. C. & Horn, R. G. The drainage of thin liquid films between solid surfaces. *J. Chem. Phys.* **83,** 5311–5324 (1985).
23. Pashley, R. M. & Israelachvili, J. N. Molecular layering of water in thin films between mica surfaces and its relation to hydration forces. *J. Colloid Interf. Sci.* **101,** 511–523 (1984).
24. Homola, A. M., Israelachvili, J. N., Gee, M. L. & McGuiggan, P. M. Measurements of and relation between the adhesion and friction of two surfaces separated by molecularly thin liquid films. *J. Tribol.* **111,** 675–682 (1989).
25. Ravina, I. & Low, P. F. Relation between swelling, water properties and b-dimension in montmorillonite-water systems. *Clays Clay Minerals* **20,** 109–123 (1972).
26. Cui, S. T., Cummings, P. T. & Cochran, H. D. Molecular simulation of the transition from liquidlike to solidlike behavior in complex fluids confined to nanoscale gaps. *J. Chem. Phys.* **114,** 7189–7195 (2001).
27. Berman, A., Drummond, C. & Israelachvili, J. Amontons' Law at the molecular level. *Tribol. Lett.* **4,** 95–101 (1998).
28. Tabor, D. & Winterton, R. H. The direct measurement of normal and retarded van der Waals forces. *Proc. R. Soc. A* **312,** 435–450 (1969).

Acknowledgements

We thank D. Chandler, J. Israelachvili, S. Safran and S. Titmuss for comments and discussions. We thank the Eshkol Foundation for a studentship (U.R.), and the US–Israel Binational science Foundation, the Deutsche–Israelische Program (DIP) and the Minerva Foundation for their support of this work.

Correspondence and requests for materials should be addressed to J.K. (e-mail: jacob.klein@weizmann.ac.il or jacob.klein@chem.ox.ac.uk).

Anomalous properties in ferroelectrics induced by atomic ordering

A. M. George, Jorge Íñiguez & L. Bellaiche

Physics Department, University of Arkansas, Fayetteville, Arkansas 72701, USA

Complex insulating perovskite alloys are of considerable technological interest because of their large dielectric and piezoelectric responses. Examples of such alloys include $(Ba_{1-x}Sr_x)TiO_3$, which has emerged as a leading candidate dielectric material for the memory-cell capacitors in dynamic random access memories[1]; and $Pb(Zr_{1-x}Ti_x)O_3$ (PZT), which is widely used in transducers and actuators[2]. The rich variety of structural phases that these alloys can exhibit, and the challenge of relating their anomalous properties to the microscopic structure, make them attractive from a fundamental point of view. Theoretical investigations of modifications to the atomic ordering of these alloys suggest the existence of further unexpected structural properties[3] and hold promise for the development of new functional materials with improved electromechanical properties. Here we report *ab initio* calculations that show that a certain class of atomic rearrangement should lead simultaneously to large electromechanical responses and to unusual structural phases in a given class of perovskite alloys. Our simulations also reveal the microscopic mechanism responsible for these anomalies.

The class of $Pb(Mg_{1/3}Nb_{2/3})O_3$–$PbTiO_3$ (PMN–PT) and $Pb(Zn_{1/3}Nb_{2/3})O_3$–$PbTiO_3$ (PZN–PT) perovskite ferroelectric alloys have been reported[4] to show remarkably large piezoelectric constants around 2,000 $pC\,N^{-1}$. These materials thus promise improvements in the resolution and range of ultrasonic and sonar listening devices[5]. Perovskite $A(B'B''\ldots)O_3$ alloys are also of great interest, as demonstrated by the discovery of an unexpected monoclinic phase[6] in $Pb(Zr_{1-x}Ti_x)O_3$. These two findings have led to a search for materials with even larger electromechanical response and/or currently unobserved phases. In particular, if a mechanism can be found that occurs in a large number of ferroelectric alloys, markedly enhances the piezoelectricity and the dielectric responses, and leads to unexpected structural features, that mechanism is likely to have large technological and fundamental implications. Here we report that such a mechanism exists and simply consists in rearranging in a certain way the atoms in a heterovalent alloy (that is, an alloy made of atoms belonging to different columns of the periodic table). More precisely, we predict that materials made of the sequences $Pb(Sc^{3+}_{0.5+p}Nb^{5+}_{0.5-p})O_3$/$Pb(Sc^{3+}_{0.5}Nb^{5+}_{0.5})O_3$/$Pb(Sc^{3+}_{0.5-p}Nb^{5+}_{0.5+p})O_3$/$Pb(Sc^{3+}_{0.5}Nb^{5+}_{0.5})O_3$ along the [001] direction should show very large electromechanical responses,